Analytical re-examination of the submerged laminar jet's velocity evolution

Barak Kashi, Elad Weinberg, and Herman D. Haustein

Citation: Physics of Fluids **30**, 063604 (2018); doi: 10.1063/1.5028560
View online: https://doi.org/10.1063/1.5028560
View Table of Contents: http://aip.scitation.org/toc/phf/30/6
Published by the American Institute of Physics

PHYSICS TODAY
WHITEPAPERS

ADVANCED LIGHT CURE ADHESIVES

Take a closer look at what these environmentally friendly adhesive systems can do

READ NOW

PRESENTED BY
MASTERBOND
ADHESIVES | SEALANTS | COATINGS

Analytical re-examination of the submerged laminar jet's velocity evolution

Barak Kashi, Elad Weinberg, and Herman D. Haustein
Faculty of Engineering, School of Mechanical Engineering, Tel-Aviv University, Ramat-Aviv, Tel-Aviv, Israel

(Received 12 March 2018; accepted 6 June 2018; published online 26 June 2018)

Understanding laminar submerged jet flight is important to many transport processes, although existing theory is insufficient within the most relevant near-nozzle region defined by the effective distance $x'/(D{\cdot}Re) < 0.05$. A linearized convection diffusion momentum equation is employed to derive an approximate flow description within the jet core, for all archetypal issuing profiles. This is validated in the core region near the nozzle by numerical simulations and experimental measurements, and it provides novel insights and adaptation of the far-field (self-similar) Schlichting jet solution. It is employed here to reveal the detailed contour of each profile's potential core and allows its differentiation from a new "boundary core" concept—the region unaffected by the change of the jet-edge shear transition from pipe flow to free-jet. This new concept reveals the minimal distance at which self-similarity can begin to exist, thereby analytically determining the virtual origin required to bring the existing far-field solution nearest to the nozzle. Thus, profile evolution and jet width become predictable within the near-nozzle region for all issuing profiles. As an alternative to the lengthy full prediction, current analysis also facilitates analytical rederivation of physically based parameters for two existing correlations describing the full uniform profile evolution and the centerline velocity decay for all other issuing profiles. *Published by AIP Publishing.* https://doi.org/10.1063/1.5028560

NOMENCLATURE

a_n	constants in the Fourier series representations of the partially developed profiles
b_n	constants in the Fourier series representations of the partially developed profiles
B	radial size of the analytical domain size
C_1, C_2, C_3	model constants
d_p	particle diameter (μm)
ϵ	cut-off value (%)
ω	base frequency in the Fourier series representations of the partially developed profiles
D	nozzle diameter (m)
f	Fourier series representations of issuing profiles
γ	exponential rate
H	nozzle to lower bounding wall distance (experiments) (m)
J	dimensionless momentum flux
l	nozzle length (m)
L_{PC}	potential core length, normalized by the nozzle diameter
L_{BC}	boundary core length, normalized by the nozzle diameter
St	Stokes number
Re	Reynolds number, based on the nozzle diameter
r'	radial coordinate (m)
r	radial coordinate, normalized by the nozzle diameter
r^*	edge of potential core in the radial direction
r_ϵ	radial jet size
ρ	fluid density (kg/m^3)
u'	axial velocity (m/s)
u	axial velocity, normalized by mean velocity
x'	stream-wise coordinate of jet flight (m)
x	stream-wise coordinate of jet flight, normalized by the nozzle diameter
Δx	virtual origin of point source jet
Z	effective nozzle length

Subscripts

BC	boundary core
m	mean
PC	potential core
SS	self-similar
approx.	approximate
uni	uniform
par	partially developed
dev	fully developed
1-3	velocity profile indices: non-monotonous, weakly developed, intermediately developed, accordingly

INTRODUCTION

Submerged jets (Fig. 1) are employed in many practical applications and processes, over a wide range of flow rates (expressed by the Reynolds number, *Re*), phases (gas-in-gas or liquid-in-liquid), and geometrical configurations (Agostini *et al.*, 2007; Carlomagno and Ianiro, 2014; Jambunathan *et al.*, 1992; Lienhard, 2006; and Viskanta, 1993). As the literature shows, many hydrodynamic aspects of submerged jets have been dealt with, often including resulting transport phenomena, such as heat transfer (Webb and Ma, 1995). Previous studies by Rohlfs *et al.*, 2012 and Kashi and Haustein, 2018 showed a direct relation between impinging jet heat transfer and near-wall jet **centerline velocity**, dictated by the hydrodynamics of issuing profiles and jet flight.

The present study, being motivated by obtaining a better understanding of the hydrodynamics and heat transfer of

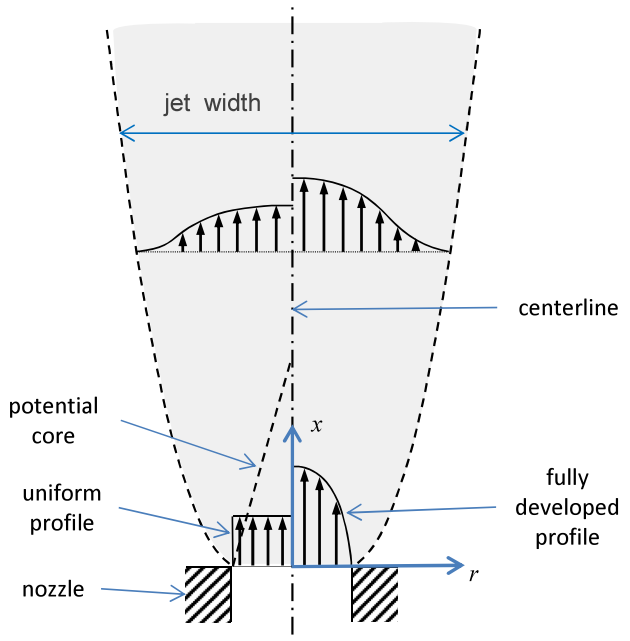

FIG. 1. Definition of free-jet zones for two extreme profiles.

micro-scale submerged jets, is focused on the laminar regime (Rosa *et al.*, 2009). Within this regime, besides the inherent characteristic scale of the jet diameter, the jet flight evolution has been shown to scale according to the effective flight distance, $x'/(D{\cdot}Re) = x/Re$ (Rankin and Sridhar, 1981), where x' is the dimensional axial coordinate, x is the axial coordinate normalized by the nozzle diameter D, and Re is the Reynolds number based on the nozzle diameter. From a practical viewpoint, the *near-nozzle* ($x/Re < 0.05$) jet flight is the most relevant—ranging from a few diameters and up to tens of diameters from the nozzle. For instance, a recent study on the diffusion of ambient species into the jet core showed full penetration within a distance of $x/Re < 0.025$ (Schmidt-Bleker *et al.*, 2014). Far from the jet axis, radial jet widening has been shown to depend on the issuing profile (Uddin and Pollard, 2007), with significant implications to the jet-to-jet interaction and parallel wall proximity (Cabaleiro *et al.*, 2015 and Herczynski *et al.*, 2004, accordingly). These recent studies should benefit from the re-examination of the near-nozzle jet flight, undertaken here.

While this region has been studied numerically and experimentally, a very few attempts have been made at obtaining a general analytical solution, providing closed-form useability, comprehensiveness, systematic methodology, and physical insight. Therein the present study focuses on the flight of a submerged jet, using analytical tools to develop improved theory and new insight for this region. The derived model is validated against comprehensive data obtained through numerical simulations, further supported by experimental measurements. Thus the present study addresses the need for more physically based models, not only for the extreme cases (uniform and parabolic profiles) but for all intermediate issuing profiles as well. The practical relevance of partially developed profiles issuing from pipe-type nozzles to heat transfer was demonstrated in a recent study by Kashi and Haustein, 2018, covering also profiles affected by the vena contracta occurring in very short pipes (orifices).

For the two extreme cases of a uniform issuing profile (Martin, 1977) and for a fully developed parabolic profile (Kneer *et al.*, 2014), simple empirical correlations exist. The latter suggested the form in Eq. (1) for the centerline velocity decay, demonstrating the importance of the effective jet flight scale, x/Re,

$$u_{\mathrm{Kneer}}(0,x) = 0.36 + 1.64 \cdot \exp(-12.6x/Re). \tag{1}$$

For the uniform issuing profile, although realizable only approximately with special nozzles (Grandchamp *et al.*, 2012), an empirical expression for high Re was suggested (Martin, 1977): Eq. (2) for the centerline velocity and Eq. (3) for the radial distribution. These expressions involve one fit parameter, proposed to be $C_1 \approx 0.1$, and L_{PC}, the generally unknown dimensionless potential core length, proposed as the location where the dynamic pressure has reduced to 95% of its initial value, giving $C_2 = 0.408$. It is shown in the following that the potential core length (uniform case) and that the fit parameters of both these models can be analytically established from physical constraints and that the range they cover can be extended, to better establish their validity in the laminar near nozzle region,

$$u_{\mathrm{Martin}}(0,x) = \left(1 - \exp\left(-\left(\frac{1}{\sqrt{2}\frac{C_2}{(L_{\mathrm{PC}}/D)}x}\right)^2\right)\right)^{1/2}, \tag{2}$$

$$\frac{u_{\mathrm{Martin}}(r,x)}{u_{\mathrm{Martin}}(0,x)} = \exp\left(-\left(\frac{r}{C_1 x}\right)^2\right). \tag{3}$$

For all profiles, existing self-similar (SS) theory for the flight of a jet originating from a point source covers only the very far-downstream region (Schlichting, 1967), suffering from singularity near the nozzle (Fig. 2). Recent attempts to adapt this existing theory include jet-startup and turbulent conditions (Cabaleiro *et al.*, 2015 and Uddin and Pollard, 2007). More relevant to present *steady laminar* jets, previous attempts (Andrade and Tsien, 1937; Revuelta *et al.*, 2002b; and 2004) have not been very successful in the truly near-nozzle region, as shown in Fig. 2(a). These studies follow the commonly accepted adaptation to the classical theory using a virtual origin, i.e., an upstream shifting of the jet's point source, giving

$$u_{\mathrm{SS}}(r,x) = \frac{3}{32}\frac{J}{\frac{x+\Delta x}{Re}\left(1 + \frac{1}{64}\frac{r^2}{((x+\Delta x)/Re)^2}\right)^2}, \tag{4}$$

where x and r are the axial and radial coordinates, respectively, normalized by the nozzle diameter D, ρ is the fluid density, and $J = \int_0^\infty u^2 r\,\mathrm{d}r$ is the dimensionless momentum flux, also known as the jet thrust (Davies *et al.*, 1977). In general, the thrust (or normalized momentum flux) increases with the level of development: from 1 for uniform up to 4/3 for fully developed, specific to each issuing profile [a result of the effective nozzle length, $l/(D{\cdot}Re)$] of the jet. This approach has been successfully employed with other self-similar solutions to extend their range of applicability: in impingement and wall jets

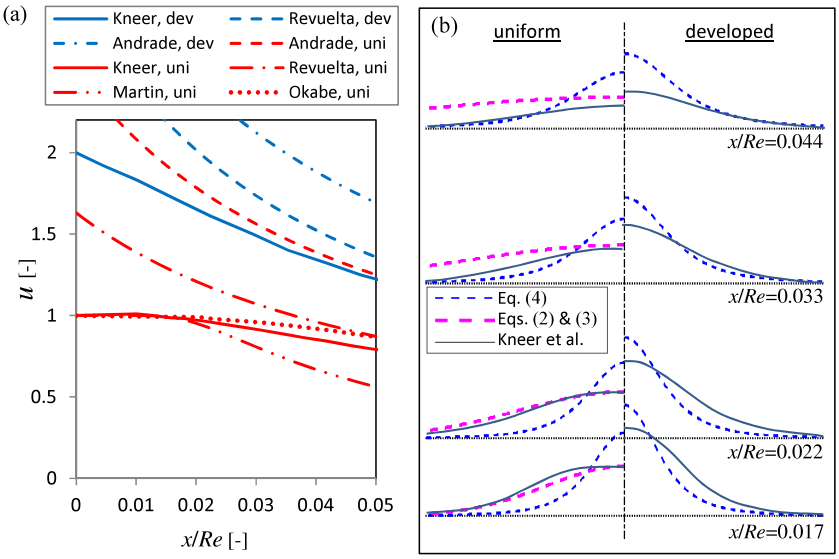

FIG. 2. Status of existing theory for uniform and developed jet flight: self-similar theory Eq. (4) + virtual origin by Andrade and Tsien/Revuelta *et al.* vs empirical correlations by Martin, Eqs. (2) and (3), or Kneer, Eq. (1), vs previous numerical results [Kneer *et al.* (2014); Okabe (1948) in Rankin and Sridhar (1981)]: (a) decay of the centerline velocity and (b) detailed velocity profile evolution.

by Glauert, 1956 and Watson, 1964, accordingly, and recently by Haustein *et al.*, 2017 and Kashi and Haustein, 2018 for jet nozzle flow.

In the notable early work of Andrade and Tsien, 1937, two competing theoretical requirements for the value of the virtual origin were considered, besides empirical fitting. The first, considering the finite size of the jet nozzle, requires that a streamline passes tangentially to the nozzle wall at the exit plane. The second addresses the non-physical infinite energy flux of the point source located at the nozzle exit plane and instead shifts the point source so that the specific profile's energy flux is obtained there. However, these authors could not resolve these competing approaches, and the value they eventually suggested ($\Delta x/Re$ = 0.04) does not successfully predict the near-nozzle jet centerline velocity or profile evolution. Later studies dealing only with the developed jet case gave empirical values in the range of $\Delta x/Re$ = 0.05-0.0625 [reviewed in Rankin and Sridhar (1981)], whereas a semi-analytical study for this case (Lee *et al.*, 1997) suggested the concept of a virtual origin *moving* across this range. In later studies by Revuelta *et al.* (2002b; 2004), perturbation methods were employed to derive a value for the virtual origin, showing asymptotic convergence to classical theory with virtual origin values similar to the aforementioned study (uniform—0.058 and parabolic—0.042). However, all these values are somewhat low and insufficient for bringing classical theory into agreement in the near-nozzle region, as defined here. In contrast to these efforts, in the present study, an analytical approximate solution is derived for the linearized convection-diffusion momentum equation—strictly valid only for near-nozzle conditions. Based on this approximate flow field description, the potential core contour is then found analytically and a novel boundary core concept is introduced. This concept reveals the minimum distance at which self-similarity can begin to exist, thereby identifying the upper bound for virtual origin values. Thus a method for finding the virtual origin values for any issuing profile is shown and demonstrated for several *archetypal* profiles—including a non-monotonic one. The validity of these newly proposed virtual origins is demonstrated through the successful prediction of the widening of the jet in the downstream half of the near-nozzle region.

The new solution derived for the *submerged* jet flight of various issuing profiles compliments a previous study by authors on *free-surface* jet flight (Haustein *et al.*, 2017). Through scale-analysis, the momentum balance equation was simplified in the vicinity of the near-nozzle jet axis. A perturbation-type profile evolution approximation was then used, resulting in a linearized convection-diffusion momentum equation, previously employed successfully for pipe flow development (Atabek, 1961) and *free-surface* jet flight (Duda and Vrentas, 1967). Its solution is of the exponential/Bessel-series type which allows any arbitrary inlet condition, i.e., any issuing velocity profile. This solution successfully approximates the evolution of the jet velocity profile within the *first half* of the near-nozzle domain ($x/Re < 0.025$), especially for $r < 1/2$. Consequently it yields the potential core contour and enables a conceptually new definition of a "boundary core," leading to the determination of the required virtual origin and its dependence on the issuing profile. Modified by this virtual origin, the self-similar theory successfully covers the *second half* of the near nozzle region.

METHODS FOR VALIDATION

The current study offers an analytical solution to the flow field in the jet core, which is validated by both numerical and experimental tools. The numerical tool and its verification are presented first, followed by a description of the experimental work and its uncertainty analysis, employed in a limited capacity for validation of the primary numerical tool.

Numerical methods

Numerical solutions of the Navier-Stokes equations were applied in this work to obtain detailed descriptions of the velocity field of free jets in the range of Re = 220–2000 as reference/validation results. Although jets typically exhibit unsteady flow, such as jet-edge vortex generation, even at moderate Reynolds numbers (Angioletti *et al.*, 2003;

Chung *et al.*, 2002; and O'Neill *et al.*, 2004), it has been demonstrated experimentally that under controlled conditions small jets can be maintained steady at $Re \cong 1400$ (Rohlfs *et al.*, 2015), agreeing with the present observations [see Fig. 6(b)]. Moreover, studying even an idealized model of a steady free-jet (submerged jet flight) can provide fundamental insights and a foundation for dealing with the unsteady aspects.

Despite the steady nature of the studied problem, to be on the safe side, the first case at $Re = 2000$ was solved using a transient solver with adaptive time-step size, where the Courant number was limited to 0.5. The flow was simulated until a steady velocity field was observed and verified, i.e., doubling the simulated flow time (to a total of 6.4 s) resulted in differences smaller than 1% in the velocity profile, even 50 diameters downstream of the nozzle. This steadiness is in agreement with a previous study by Kashi and Haustein, 2018 and the present experimental observations. Therefore, subsequent cases were solved using a steady-state solver, without perceivable convergence issues.

The numerical models in the present study were solved using the finite volume open-source CFD code OpenFOAM (Greenshields and Weller, 2010), where velocity-pressure coupling was dealt with using the SIMPLE algorithm with the convergence criteria set to residuals below 10^{-4}.

The numerical model consisted of an axisymmetric domain spanning 60 and 12 jet diameters in the stream-wise and radial directions, respectively (Fig. 3). A vertical inlet was positioned at the origin, followed by a stationary wall in the same direction. The other two boundaries were of the inlet/outlet type, where the Neumann pressure condition is applied for outflow and the Dirichlet condition for velocity inflow.

At the inlet, different realistic velocity profiles were imposed, previously obtained in a nozzle flow study by Kashi and Haustein, 2018, shown in Fig. 4: (1) a uniform profile, denoted *uni*; (2) three partially developed profiles, denoted *par* 1, *par* 2, and *par* 3, corresponding to nozzle lengths of $Z = l/(D{\cdot}Re) = 0.0005$, 0.003, and 0.01, accordingly, where l is the nozzle length and D is the nozzle diameter; and (3) a fully developed profile, denoted *dev*. Note that the least developed velocity profile (*par* 1) features an off-center peak (indicated by a green arrow), which is a result of the vena contracta phenomenon typical to short nozzles ($l/D = 1/4$). These profiles are adapted for the analytical solution in Appendix B, where the partially developed ones are approximated by the Fourier series.

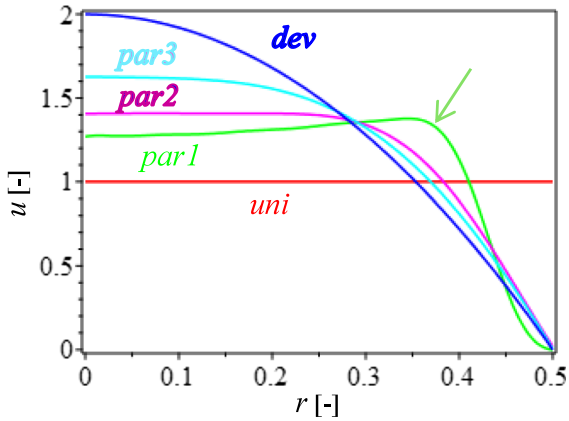

FIG. 4. Issuing profiles considered, taken from previous simulations [Kashi and Haustein (2018)]: *par* 1, *par* 2, and *par* 3, corresponding to nozzle lengths of $Z = l/(D{\cdot}Re) = 0.0005$, 0.003, and 0.01, accordingly.

The numerical domain was meshed with quadratic cells of varying cell size: In the x-direction, cells had a 1:3 growth ratio, while in the r-direction, a 2:1 ratio was used for $r \le D/2$ and a 1:14 ratio for $r > D/2$. The final working mesh consisted of 80 000 cells for all issuing profiles and all Re. However, more extensive cases were run for mesh and domain size independence tests detailed in Appendix A.

The present numerical results were also thoroughly validated in the section titled Results, by comparison of the following: (1) uniform and developed profiles with previous numerical results (Fig. 7), (2) centerline velocity decay for the developed issuing profile with present experimental results, and (3) velocity profiles at five axial locations with present experimental results (Fig. 13).

Experimental methods

To further validate the numerical simulations and better establish the existing and modified theory, detailed flow field experimental measurements were conducted. Flow field visualization was based on the well-established quantitative method of shadow-type micro-PIV (particle image velocimetry, Cummings, 2000).

The system employed for these measurements is shown in Fig. 5 and consists of a standard open loop flow pathway. The flow contains a small fraction of particles so as not to affect

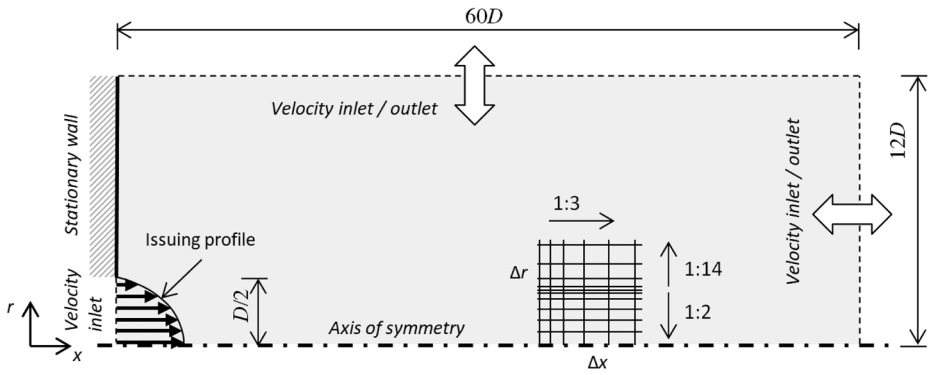

FIG. 3. The numerical model: geometry, mesh, and boundary conditions.

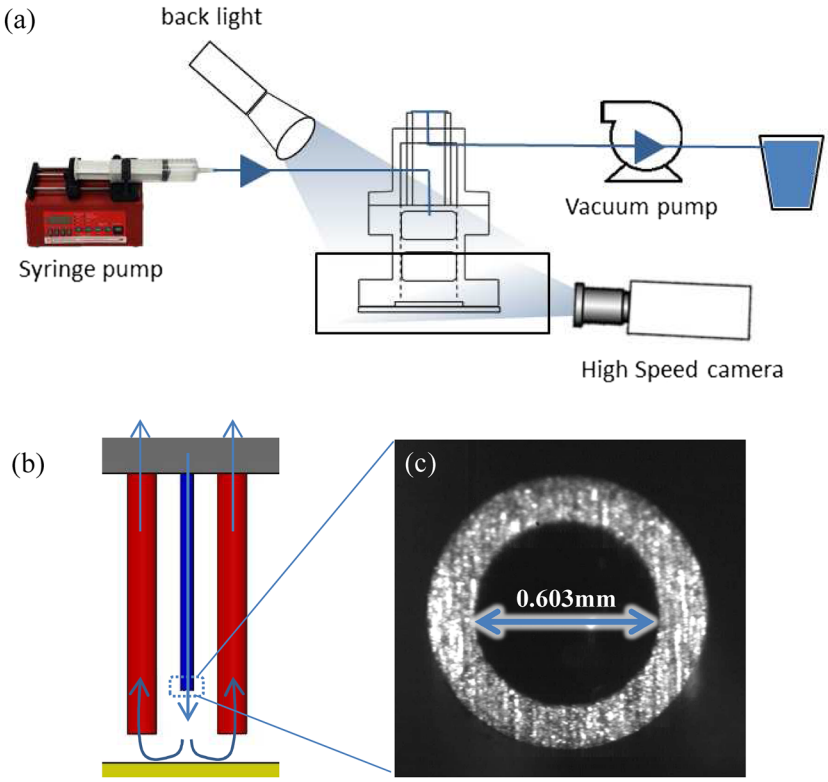

FIG. 5. Experimental setup: (a) system schematic; (b) close-up view of the test section; (c) micrograph verifying jet nozzle precision.

liquid properties (<0.03% solid load), namely, soda-lime glass microspheres with a particle diameter distribution of $d_p(10\%) \leq 2\ \mu$m, $d_p(50\%) \leq 3\ \mu$m, and $d_p(90\%) \leq 7\ \mu$m. This results in a typical Stokes number of $\mathrm{St} = \rho_p d_p{}^2 \mathrm{Re}/(18\rho D^2) \cong 0.01$, which guarantees excellent flow tracking of the tracer particles (Tropea and Yarin, 2007). The particle-laden flow was driven by an accurate syringe pump (model NE1010, 10 μl/min resolution), giving a flow calibrated by high-sensitivity scale tests to within ±1%. On the outflow side, a Venturi-type vacuum pump driven by compressed air was used to steadily extract spent liquid under weak vacuum (~0.8 atm absolute). The test section housing is from polished PMMA (polymethyl methacrylate), chosen for its transparency and refractive index proximity to the working liquid—de-ionized water. This housing held the submerged pipe-type jet (drawn stainless steel flat-end needle with $l/D = 71$, $D = 0.603$ mm) within a controlled environment (bath)—shown in Figs. 5(a) and 5(b). The accurate jet tube, verified under a microscope [Fig. 5(c)], was long and smooth and therefore able to closely reproduce the fully developed (parabolic) issuing profile, up to $Re \cong 1500$. The jet was permitted a relatively long flight (up to 20 diameters, micrometrically adjustable) eventually impinging on the transparent bottom plate—from there flowing radially outward to four extraction nozzles (1.2 mm diameter, 35D long) located 5D downstream of impingement.

Several measurements were made: pressure drop through the system, inlet and outlet temperature (by PT100 DIN 1/3, pre-calibrated to ±0.1 °C), and high speed photography for PIV with focused light-emitting diode (LED) lighting. The latter employs a Phantom v12.1 camera, with a long working distance microscope, Navitar ×12 lens. Typical magnification in the range of X4-X9 gave a resolution of 5-2.2 μm/pix, with a typical depth of correlation (effective depth of field) of 135 μm [calculated according to Olsen (2010)]. Exposure duration was set to 6 μs to avoid motion blur, and the frame rate was set proportional to Re in the range of 16 000-36 000 fps to capture the instantaneous flow. For the PIV analysis, relatively small interrogation windows with few particles were employed (15 μm × 15 μm, with an overlap of around 20%) over a long time period ~1 s, in order to obtain sufficient data from the steady flow. These settings and methods gave uncertainty in measured velocity values of less than 8%. Typical raw data obtained by the system are shown in Fig. 6, which underwent enhancement [e.g., background subtraction shown in Fig. 6(a)] for better analysis in the PYTHON-based PIV open-source software used (Allan *et al.*, 2015). Long duration particle tracking over a few seconds gave clear pathline images [Fig. 6(b)] indicating a steady flow, with no jet edge vortices. This steadiness was clearly observed up to $Re = 1000$, while images at higher Re were noisier though still without distinct jet-edge vortices attributed to a smooth/controlled system—in agreement with other small-scale experimental studies (Rohlfs *et al.*, 2015). Figure 6(c) shows a validation of the PIV results obtained by the method described, through comparison of the profile obtained near the nozzle with the theoretical issuing profile (Poiseuille flow).

In the light of the quasi-steady nature of the flow analyzed here, PIV data for velocity profiles were obtained over several thousand frames (typically >4000), permitting acquisition of extensive velocity data over relatively long periods. Furthermore, to avoid an artificial bias of the results,

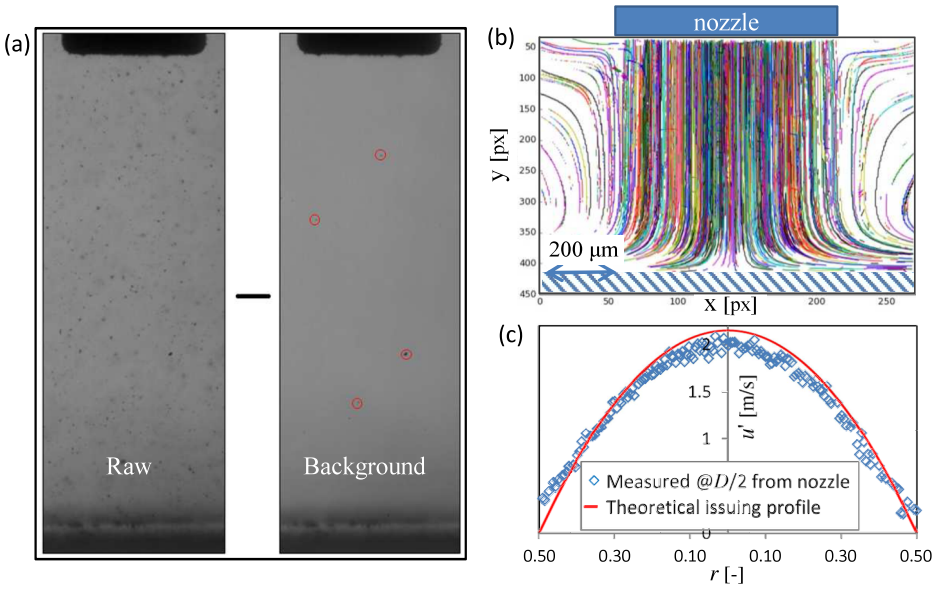

FIG. 6. PIV raw data: (a) raw images and background used for subtraction to remove constant noise; (b) long duration measurement pathlines, Re = 500 and H/D = 2; (c) raw data—post-initial filtration and comparison to the initial issuing profile.

out-of-plane velocity data were filtered out, as they could be identified as the lowest 10% of values in each interrogation window.

JET FLIGHT APPROXIMATE SOLUTION

General derivation

In the present study, an analytical approach was taken and an approximate solution to the governing equations was sought. This was done with the purpose of identifying the contribution of the dominant physical mechanisms, while neglecting small scale terms in order to obtain the solution analytically.

The axisymmetric non-dimensional Navier-Stokes equation in the axial direction is

$$v\frac{\partial u}{\partial r}+u\frac{\partial u}{\partial x}=\frac{1}{Re}\left(\frac{1}{r}\frac{\partial}{\partial r}\left(r\frac{\partial u}{\partial r}\right)+\frac{\partial^2 u}{\partial x^2}\right), \tag{5}$$

where r is the radial coordinate normalized by the nozzle diameter and u and v are the velocity in the axial and radial directions, respectively, normalized by the issuing jet mean velocity. As Eq. (5) is not analytically solvable, it is approximated by analysis only near the jet axis and within the near nozzle region.

Since as $r \to 0$, $v \to 0$, and $\mathrm{d}u/\mathrm{d}r \to 0$, near the jet axis

$$v\frac{\partial u}{\partial r} \ll u\frac{\partial u}{\partial x}. \tag{6}$$

Additionally, since $Re \gg 1$, and for $x > 1$, $u \sim 1$, it can be claimed that $\frac{1}{\mathrm{Re}}\frac{\partial^2 u}{\partial x^2} \ll u\frac{\partial u}{\partial x}$; i.e., the axial diffusion term can be neglected relative to axial convection, as is typically done by Hennecke, 1968, thus arriving at

$$u\frac{\partial u}{\partial x}=\frac{1}{Re}\frac{1}{r}\frac{\partial}{\partial r}\left(r\frac{\partial u}{\partial r}\right). \tag{7}$$

As this equation is still non-linear, we define the velocity as a perturbation u_{per} around the centerline value $u_{(0,0)}$, giving $u = u_{(0,0)} + u_{\mathrm{per}}$. Substituting this into Eq. (7) gives

$$\frac{1}{2}\frac{\partial\left(u_{(0,0)}^2+2u_{(0,0)}u_{\mathrm{per}}+u_{\mathrm{per}}^2\right)}{\partial x}=u_{(0,0)}\frac{\partial u_{\mathrm{per}}}{\partial x}. \tag{8}$$

As the approximation requires $u_{\mathrm{per}} \ll 1$, it is strictly valid only near the jet axis and for short flight distances—about halfway through the near nozzle region.

For $u_{(0,0)} \sim 1$ and $u_{\mathrm{per}} \ll 1$, we get

$$u_{(0,0)}\frac{\partial u_{\mathrm{per}}}{\partial x}=\frac{1}{Re}\frac{1}{r}\frac{\partial}{\partial r}\left(r\frac{\partial u_{\mathrm{per}}}{\partial \mathrm{r}}\right). \tag{9}$$

A more quantitative range of validity is seen to be $r < 0.16$-0.5 depending on the initial profile and in the axial direction not far beyond the potential core length, defined as the point on the centerline where the pressure drops below 95% of its initial value (Martin, 1977), or the velocity at the centerline is yet unaffected by the shear layer (Incropera *et al.*, 2011; Or *et al.*, 2011; and Zuckerman and Lior, 2006). Although this linearization is not easily justified for non-uniform profiles, as evident in Fig. 2(b), near the axis, the deviation from the initial velocity profile is small, a matter which will be further considered in the section titled Results. This simplification of the steady Eulerian Navier-Stokes equations is similar to the linearization performed in pipe flow development (Atabek, 1961) and free-surface jet flight (Duda and Vrentas, 1967). Similar to these studies, the present study finds approximate closed-form solutions, much preferable to those found through the more complex Lagrangian approach, attempted only for *developed* submerged jets (Lee *et al.*, 1997).

Reintroducing the definition $u_{\mathrm{per}} = u_{(0,0)} - u$ into Eq. (9) gives

$$u_{(0,0)}\frac{\partial u}{\partial x}=\frac{1}{Re}\frac{1}{r}\frac{\partial}{\partial r}\left(r\frac{\partial u}{\partial \mathrm{r}}\right), \tag{10}$$

with the boundary condition of $u_{(B,x)} = 0$ and $\partial u_{(0,x)}/\partial r = 0$, where B is the radial domain size, determined in Appendix B (see Fig. 18).

The solution for this linear ordinary differential equation (ODE) is well known and has the form (Carslaw and Jaeger, 1959)

$$u(r,x) = \frac{2}{B^2}\sum_{n=1}^{\infty}\frac{J_0(\beta_n r)}{J_1^2(\beta_n B)}\exp\left(-\frac{\beta_n^2 x}{u_{(0,0)}Re}\right) \times \int_0^B r' J_0(\beta_n r') f(r')\mathrm{d}r', \tag{11}$$

where J_0 and J_1 are the first-kind Bessel functions of order 0 and 1, respectively, $f(r)$ is the issuing velocity profile (equal to unity for the uniform case), and β_n are solutions of

$$J_0(\beta_n B) = 0. \tag{12}$$

While this approximate analysis was conducted for the simpler case of a uniform issuing velocity profile, easily described by small perturbations around a mean, its applicability is examined here for all profiles mentioned in the subsection titled Numerical methods (shown in Fig. 4). A verification of the solution given in Eq. (11), very near the exit from the nozzle ($x = 0.1$) for all issuing velocity profiles considered, by means of a truncated series and within a finite domain, is detailed in Appendix B.

The uniform case model

Motivated by the mathematical inconvenience involved in resolving the uniform profile and armed with a new analytical derivation for the velocity profile evolution near the core, it is possible to predict the potential core length (discussed extensively around Fig. 9), and we now employ the well-known jet momentum conservation assumption to treat an existing empirical uniform profile model.

This model is dealt with in two distinct regions—within the potential core and beyond it. Within the latter region ($x > L_{PC}$), the requirement to conserve jet momentum flux, using Eqs. (2) and (3), can be written as

$$\int_0^{\infty} 2\pi\rho r\left(u_m \exp\left(-\left(\frac{r}{C_1 x}\right)^2\right)\sqrt{1-\exp\left(-\left(\frac{1}{\sqrt{2}C_2 x}\right)^2\right)}\right)^2 \mathrm{d}r = \int_0^{D/2} 2\pi\rho r u_m^2 \mathrm{d}r, \tag{13}$$

where $u_m = 1$ is the mean issuing velocity to obtain a closed-form expression for C_1 that guarantees conservation of momentum,

$$C_1|_{x>L_{PC}} = \frac{\sqrt{2}}{2x\left(1-\exp\left(-3.004\frac{L_{PC}^2}{x^2}\right)\right)^{1/4}}. \tag{14}$$

By contrast, for $x \le L_{PC}$, within the potential core, the radial integration is performed in a piece-wise manner—within the core and outside of it. As the inner part of the integration, i.e., the unaffected velocity, cancels out, the momentum flux conservation requirement becomes

$$\int_{r_{PC}D}^{\infty} 2\pi\rho r\left(u_m \exp\left(-\left(\frac{r-r_{PC}}{C_1 x}\right)^2\right)\right)^2 \mathrm{d}r = \int_{r_{PC}D}^{D/2} 2\pi\rho r u_m^2 \mathrm{d}r, \tag{15}$$

where r_{PC} is the radial edge of the potential core, conveniently approximated by the commonly accepted linear relation [also termed a *quasi-conical* domain in Carlomagno and Ianiro (2014)]

$$r_{PC} = \frac{1}{2}\left(1-\frac{x}{L_{PC}}\right) \tag{16}$$

employed for the integration to obtain

$$C_1|_{x<L_{PC}} = \frac{\sqrt{2}}{4xL_{PC}}\left[\sqrt{\pi}(x-L_{PC}) + \sqrt{\pi(x-L_{PC})^2 - 4x(x-2L_{PC})}\right]. \tag{17}$$

Examining the uniform issuing profile case using the approximate solution for free-jet flight [Eq. (11)], we observe that at $x/Re = 0.0167$, $u_{(0,x)} = 0.95^{0.5}u_{(0,0)}$, which is the effective potential core length for this case, L_{PC}/Re. Substituting Eqs. (14) and (17) together with $L_{PC} = 0.0167\mathrm{Re}$ in Eqs. (2) and (3), we eliminate the use of all arbitrary values to obtain for the centerline velocity decay of the uniform case,

$$u_{\mathrm{Martin}}(r,x) = \left(1-\exp\left(-\left(\frac{Re}{24.2\sqrt{2}x}\right)^2\right)\right)^{1/2} \times \exp\left(\begin{cases} -\dfrac{0.002\,28 r^2 Re^2}{\left[\sqrt{\pi}(x-0.0167Re)+\sqrt{\pi(x-0.0167Re)^2-4x(x-2\times0.0167Re)}\right]^2}, & x \le L_{PC} \\ -2r^2\sqrt{1-\exp(-0.000\,858Re^2/x^2)}, & x > L_{PC} \end{cases}\right). \tag{18}$$

A simple centerline model

A previous numerical study (Kneer *et al.*, 2014) showed that at short flight distances of approximately $x/Re < 0.03$, submerged and free-surface jets have very similar decay of the centerline velocity. This can be attributed to the fact that in both cases, velocity profile relaxation is the major mechanism that moderates the centerline velocity, while shear forces with the ambient fluid affect the outer regions of the jet only reaching the core farther downstream. For the free-surface jet, a

generalized semi-analytical expression has been derived (Haustein *et al.*, 2017) in the form of an exponential decay from the initial centerline velocity $u_{(0,0)}$ to the final $u_{(0,\infty)}$, at a rate of $\gamma = 51.5$. In the submerged jet case, as the centerline velocity decays to zero, the self-similar Schlichting's jet behavior is reached at very long flight distances, where the exponential type decay transitions to the Schlichting hyperbolic decay. This point of transition is the point at which Schlichting's solution agrees [to within $0.95^{1/2}\ u_{(0,0)}$] with simulations at larger flight distances than considered here (Revuelta *et al.*, 2002b), occurring when $u \cong 0.34$ [vs. the previous empirical constant 0.36 in Eq. (1)]. The effective rate of the centerline velocity decay in a submerged jet can be found by comparison to the aforementioned model for free-surface jets [RHS of Eq. (19)], at the location where the jet centerline becomes affected by the shear layer at L_{BC}. This requirement leads to a centerline decay rate for the submerged jet of $C_3 \cong 12$ [vs the previous empirical decay rate of 12.6 in Eq. (1)], found by the comparison at a newly identified location, $L_{BC}/Re = 0.0226$, further explained in the subsection titled Boundary core, resulting in

$$\begin{aligned} &2 + (0.34 - 2)\left(1 - \exp\left(-C_3 \frac{L_{BC}}{\mathrm{Re}}\right)\right) \\ &\quad = 2 + (1 - 2)\left(1 - \exp\left(-51.5 \frac{L_{BC}}{\mathrm{Re}}\right)\right) \\ &\qquad + \left(\frac{1 + \sqrt{3/4}}{2} - \frac{1 - \sqrt{3/4}}{2} \tanh\left(0.64 \ln \frac{L_{BC}}{0.0038}\right)\right)^{-2}. \end{aligned} \tag{19}$$

Other issuing profiles (partially developed) may feature a potential core, where the centerline velocity remains constant up to L_{PC}. In such cases, the exponential decay rule can be applied after this length, giving the form

$$u_{(0,x)} = u_{(0,0)} + (0.34 - u_{(0,0)})\left(1 - \exp\left(-12 \frac{x - L_{PC}}{\mathrm{Re}}\right)\right). \tag{20}$$

Use of the values obtained through Eq. (19) for all other velocity profiles in Eq. (20) implies that the dominant mechanism is the same, i.e., an exponential type decay due to momentum diffusion away from the axis, beyond the potential core.

RESULTS

The new analytical model for laminar free-jet flight ($Re = 220$–2000) at application relevant flight distances ($x/Re < 0.05$) is validated and evaluated in a quantitative way, by comparison to previous and current numerical and experimental results. In addition, it serves to modifying existing theory and sheds new light on the jet core region. The propagation of submerged free-jets in a stagnant medium was characterized in terms of the centerline velocity, velocity profile evolution, and radial spread (jet widening), for the most relevant issuing profiles: uniform, vena-contracta affected, partially developed, and fully developed pipe flow type. In addition, the potential core contour was found for all profiles, and a conceptually new alternative was proposed.

Centerline velocity

As the first step, the numerical and experimental evaluation tools employed were established and validated by comparison to the literature. Figure 7 shows very good agreement between current experimental and numerical centerline velocities for the developed profile with previous numerical and empirical results (Kneer *et al.*, 2014 and Rohlfs *et al.*, 2014) and present numerical velocities for a uniform issuing profile with previous numerical results (Rohlfs *et al.*, 2014). Moreover, both numerical and experimental results covering a wide range of Reynolds numbers (220, 375, 500, and 2000) coincide undiscernibly when scaled over effective flight distance, x/Re, showing the independence from Re with this scaling. This agreement between experiments and simulations and Re independence with correct scaling are further demonstrated in the detailed velocity profile evolution (Fig. 13).

With the present numerical and experimental methods established as a faithful representation of jet hydrodynamics, it was possible to employ them further for the evaluation of the approximate solution. Figure 8 shows the prediction of the centerline velocity for all considered issuing profiles using Eqs. (11) and (12), with profiles defined in Appendix B, which compares quite well with the numerical results. Particularly, Fig. 8 shows the high level of accuracy with which the new model predicts the centerline velocity at the very short flight distances of $x/Re < 0.02$, the exact conditions under which it was developed. Most significantly, it is able to correctly predict the non-monotonous curve of the very-short nozzle (vena contracta affected) *par* 1 case. This initial centerline velocity rise in non-monotonous issuing profiles has previously been shown to exist both experimentally and numerically (Akaike and Nemoto, 1988 and Kashi and Haustein, 2018).

With the indication that the approximate solution is able to deal with various profiles in the jet core region near the nozzle, in the following, other jet characteristics are analyzed and new insight is gained through it. Moreover, this analysis

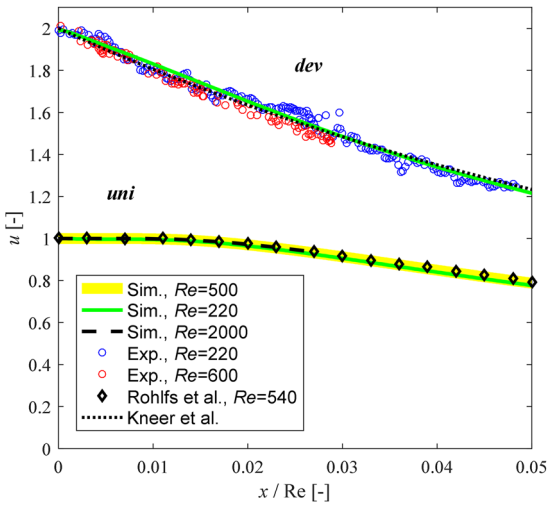

FIG. 7. Centerline velocity decay for uniform and fully developed profiles: comparison of present numerical (solid lines) and experimental results (circles) to previous numerical results [diamonds, Rohlfs *et al.* (2014)] and a subsequent correlation [dotted line, Kneer *et al.* (2014)].

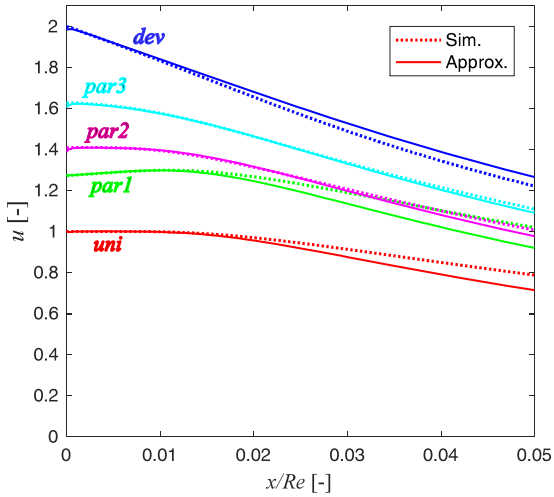

FIG. 8. Predicted decay of the centerline velocity for all issuing profiles (detailed in the caption of Fig. 4) using the approximate solution [Eqs. (11) and (12)] vs the validated simulation results.

is supported by comparison to numerical simulations, where possible.

Potential core

The classic potential core is defined as the domain in which the *velocity's magnitude* is yet unaffected by the jet-edge shear layer, usually drawn as a straight line from the edge of the nozzle to the farthest point on the centerline where the pressure maintains 95% of its initial value (Martin, 1977) or the centerline velocity drops to 99% of its initial value (Incropera *et al.*, 2011; Or *et al.*, 2011; and Zuckerman and Lior, 2006).

The classic potential core contour is found for all considered profiles (except the fully developed one, in which it is negligible), using Eq. (11), with required roots and initial conditions from Eq. (12) and profiles defined in Appendix B, accordingly. This solution is implemented by marching in x and implicitly solving for r with the requirement $u(r, x) = 0.95^{1/2}u(0, 0)$ at each axial position to obtain $r^*(x)$—the edge of the potential core. This cut-off velocity value $[0.95^{1/2}u(0, 0)]$ was suggested by Martin (1977). From searching the literature, only two numerical descriptions of the potential core contour were found: for the fully developed case and for a short nozzle with a unique inlet [Fig. 2(a) in Rohlfs *et al.* (2014) and Fig. 15 in Akaike and Nemoto (1988), accordingly]. Due to differing conditions and potential core edge criteria, a quantitative comparison is irrelevant, although Fig. 9 shows qualitative agreement with the present findings.

Figure 9(a) compares several contours of the uniform profile potential core: the common depiction of a straight-lined potential core defined according to an accepted criterion—95% of initial pressure, equivalent to 97.5% of initial velocity, the contour predicted by the approximate solution developed here and the corresponding curve from the numerical results, based on the latter criterion, as well as a depiction of this contour based on a different criterion (95% of initial velocity) from a previous study by one of the authors in the work of Kneer *et al.*, 2014. As Fig. 9(a) shows, the approximate solution reproduces the shape of the potential core, found through numerical simulation, while only deviating slightly from it in the axial direction (<10%). The deviation appears to be the lack of a stretching in the axial direction, which may be explained as being due to the neglected radial velocity in the approximate solution. In other words, continuity dictates that due to the axial deceleration within the jet there exists a weak outward radial velocity, which is expected to delay the diffusion of the effect of the momentum deficit due to the shear boundary condition toward the axis, not accounted for in the approximate solution. Furthermore, as the figure shows, the potential core contour is concave near the nozzle and becomes convex farther downstream, clearly different from the commonly used linear depiction. Moreover, remembering that the axial velocity of the profile at the edge of the potential core is constant (equal to 97.5% of the initial value), it is understood that this contour represents the local radial momentum diffusion rate. The shape of the contour shows that the rate is not constant: initially at the edge of the jet, where the curvature is very small, propagation proceeds similar to diffusion into a semi-infinite domain ($r \sim \sqrt{t} \sim \sqrt{x}$), while near the axis, as the curvature becomes significant, diffusion accelerates according to the well-known cylindrical quenching problem (Incropera *et al.*, 2011). This explanation of a transition between a falling rate to an increasing one dictates the existence of an inflection point, observable around $r = 0.2$.

Figure 9(b) shows the potential core contour predicted by the approximate solution for all issuing profiles, except for the negligible fully developed one. It clearly shows that for the monotonous profiles (excluding *par* 1) the length of the potential core is inversely proportional to the level of development within the nozzle of the issuing profile. For

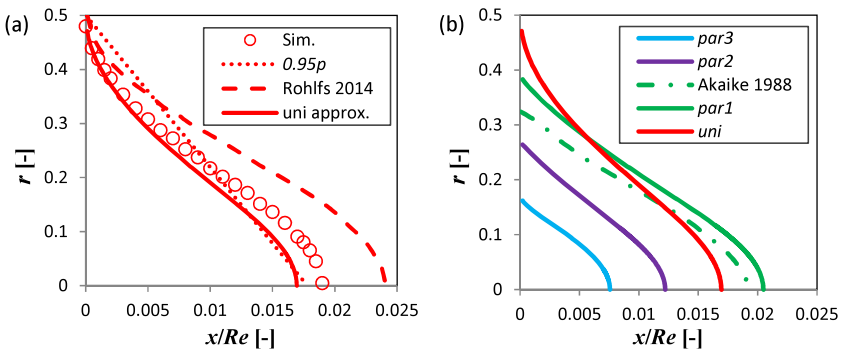

FIG. 9. Potential core contour for all issuing profiles found by the approximate method [Eq. (11)]: (a) comparison of different methods for the uniform profile and (b) contours for various profiles.

par 1—a profile which emerges from a very short nozzle and features an off-center peak caused by the extra-nozzle vena contracta (Kashi and Haustein, 2018)—relaxation drives an initial centerline velocity increase, followed by the familiar decrease, thereby leading to a longer potential core [shown as qualitatively similar to the profile in Akaike and Nemoto (1988)].

Boundary core

While this *velocity magnitude* based potential core definition is suitable for representing a uniform velocity profile, it is insufficient to describe intermediate or fully developed profiles, which begin to undergo relaxation upon emergence, due to the sudden loss of driving pressure gradient, but prior to being affected by the jet-edge shear boundary condition. This distinction from the velocity magnitude definition of the potential core was raised in a recent review by Carlomagno and Ianiro, 2014: "...the flow interior remains initially unaffected by the momentum transfer... the jet may undergo velocity variations there only as a result of velocity gradients already existing at the nozzle exit," i.e., profile relaxation. This domain is similar, although not as limited as the "parabolic core" term from the analysis of Lee *et al.* (1997). To generalize this concept, we propose here a new definition for the boundary unaffected domain, later shown to serve the quantification of each profile's virtual origin, i.e., modification required to existing self-similar theory.

As the jet emerges from the nozzle, a sudden change in the boundary condition at $r = D/2$ occurs: the no-slip condition on the nozzle wall disappears and is replaced by the new shear condition with the surrounding unbounded stagnant fluid. The information regarding this new jet-edge condition then propagates toward the jet center. It is assumed, in line with the analysis presented earlier, that this information *diffuses* radially toward the centerline, while it is *convected* downstream—following a similarity solution for *free-surface* jets (Wilson, 1986). As the diffusive progress of this information is independent of the size of the disturbance or of the initial conditions, it is suggested that the time to reach the centerline is equal for all issuing profiles. In other words, this analysis relies on a spatial decoupling, due to transfer mechanisms—radially by diffusion and axially by convection. Hence, while the signal propagates radially regardless of the issuing profile, the distance it travels axially is strongly dependent on it. The domain oblivious to the jet-edge shear boundary condition change is hereby termed the "**boundary core**."

The radial propagation **in time**, assumed to be common to all profiles, is derived from the unique case of the uniform velocity profile using the transformation $t = x/u$ to obtain $r(t)$. This specific profile is chosen, since its boundary core coincides with its potential core, and as $u = 1$, $r(t)$ can be easily transformed to $r(x)$ – the solid line shown in Fig. 9(a).

For all profiles, $x(t)$ is obtained by solving Eq. (21) along with Eq. (11), by discrete time stepping, using the function $r(t)$, common to all profiles,

$$x_{i+1} = x_i + u(r(t_i), x_i) \cdot (t_{i+1} - t_i). \tag{21}$$

Once both $r(t)$ and $x(t)$ are found, the path of the signal can be uniquely reconstructed, and the axial position where the signal arrives at $r = 0$, the boundary core length, L_{BC}, can be determined for every issuing profile, as shown in Fig. 10. In addition, while the shape of the boundary core qualitatively resembles that of the potential core, it only coincides with it in value for the case of a uniform profile. Most significantly, for this newly defined boundary domain, the dependence on the level of initial profile development is opposite to that of the potential core: the boundary core length increases with the development level from $L_{BC} = 0.0167$ for the uniform case to $L_{BC} = 0.0226$ for the fully developed one. This trend can intuitively be appreciated by considering the radial distribution of axial velocity in each profile: the more developed profiles have significantly higher velocities than the uniform one in the inner core—transporting the information of boundary shear alteration farther downstream and vice versa in the outer core. The values are similar to those found in a recent numerical study on ambient species diffusion into the jet core (Schmidt-Bleker *et al.*, 2014).

It is interesting to note that although the profiles *par* 1 and *par* 2 have quantitatively different initial centerline velocities, their resulting boundary core shapes and lengths are very similar.

The present analysis has assumed a decoupling between the profile relaxation process, beginning as soon as the jet emerges and loses its driving pressure, and the time of arrival of the jet edge shear condition (from no-slip in the nozzle to shear with the unbounded ambient fluid). Therein the boundary core as defined here addresses the latter and depicts the spatial propagation of the signal originating at the nozzle edge. This understanding suggests that a free-surface jet may exhibit similar behavior to a submerged one, within the boundary core—as is shown by the close agreement of the centerline velocity decay curves of both types for a fully developed profile in the work of Kneer *et al.* (2014). This similarity is used here to develop the simple centerline velocity decay relation for all issuing profiles, Eq. (20).

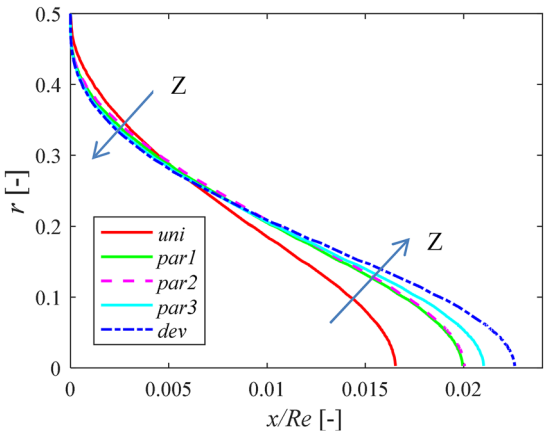

FIG. 10. The boundary core contour for all issuing profiles: $L_{BC} = 0.0167$, 0.0199, 0.0201, 0.0210, and 0.0226 for the uniform (*uni*), $Z = 0.0005$ (*par* 1), $Z = 0.003$ (*par* 2), $Z = 0.01$ (*par* 3), and fully developed (*dev*) issuing profiles, respectively.

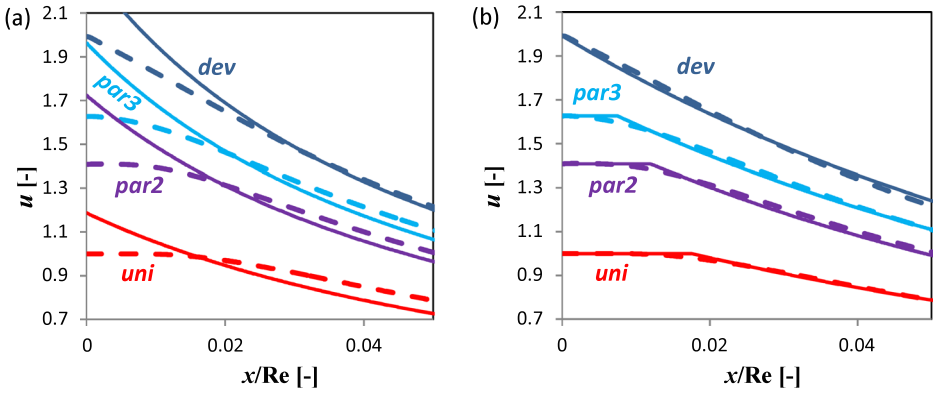

FIG. 11. Prediction of centerline velocity decay with an effective flight distance for the uniform, monotonous partially developed, and fully developed profiles vs the numerical results: (a) the shifted self-similarity solution [Eq. (4)] and (b) the centerline model [Eq. (20)].

Virtual origin

Building on the flow development occurring within the newly proposed concept of the boundary core, it is understood that self-similarity of the velocity profile cannot exist there and begins somewhat beyond its edge, after a short transition zone [see, e.g., Donaldson and Snedeker (1971)]. As not much is known of the length of the transition zone, the edge of the boundary core is used here to set the location of the virtual origin. Namely, Δx is derived from requiring equality between the centerline velocity values predicted by Eq. (11) and by Eq. (4) (shown in Fig. 8) at L_{BC}, the boundary core length shown in Fig. 10 and defined in Eq. (22). This approach is a novel alternative to previous derivations of the virtual origin (Andrade and Tsien, 1937; Revuelta *et al.*, 2002b; and 2004), given by

$$u_{SS}(0, L_{BC} + \Delta x) = u_{approx.}(0, L_{BC}). \tag{22}$$

The resulting virtual origins for the uniform (*uni*) through the three partially developed (*par* 1, *par* 2, and *par* 3) to the fully developed (*dev*) cases are $\Delta x_{uni}/Re = 0.079$, $\Delta x_{par1}/Re = 0.073$, $\Delta x_{par2}/Re = 0.068$, $\Delta x_{par3}/Re = 0.058$, and $\Delta x_{dev}/Re = 0.054$. Note that the first and last extreme values are in reasonable agreement with those obtained in previous studies (Andrade and Tsien, 1937; Lee *et al.*, 1997; Rankin and Sridhar, 1981; Revuelta *et al.*, 2002b; and 2004). These values lead to improved applicability of the theory in the near-nozzle range, demonstrated by successful prediction of the centerline velocity in Fig. 11(a). Moreover, these virtual origins were obtained analytically and in a straightforward, if somewhat lengthy, manner that can be applied to any issuing velocity profile. However, application of the larger virtual origins found in this way further impedes the downstream convergence to the self-similar solution and should therefore be used with caution and only within the region delimited here. Alternatively, if only the centerline velocity is needed and not the full profile evolution (given by the self-similar theory + virtual origin), the physically based simple model, Eq. (20), can be successfully used [see agreement in Fig. 11(b)], for any profile where the potential core is known or can be found as demonstrated in Fig. 9(a).

Figure 12 summarizes the trends of the potential core length, boundary core length, and virtual origin distance as a function of the issuing profile's jet thrust. However, the non-monotonous profile (*par* 1) deviates from this trend, as it has a high momentum despite a low level of development—affected by a vena contracta when emerging from a very short nozzle. It is interesting to note that the boundary and potential core lengths for this profile coincide—similar to the uniform profile, possibly due to its initial similarity to it. It is evident from Fig. 12(a) that the boundary core length is linearly correlated to the profile's momentum flux and that the potential core follows an opposite trend. In terms of the potential core, the non-monotonous profile (*par* 1) is seen to deviate strongly from the general trend, which does not occur in boundary core terms. In addition, as seen in Fig. 12(b), the virtual origin roughly follows a decreasing trend with an increase in momentum for all profiles—previously shown only for the extreme cases (uniform and fully developed). Thereby the direct relation

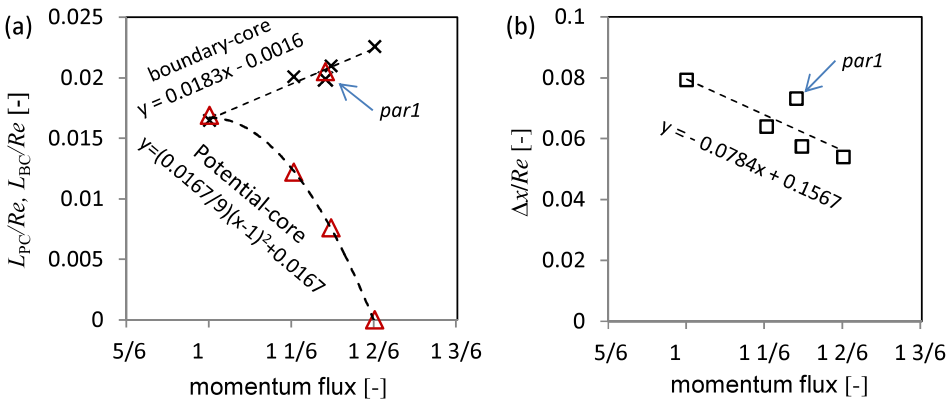

FIG. 12. Dependence of key lengths on issuing profile's momentum flux (jet thrust): (a) the potential core and boundary core and (b) the virtual origin.

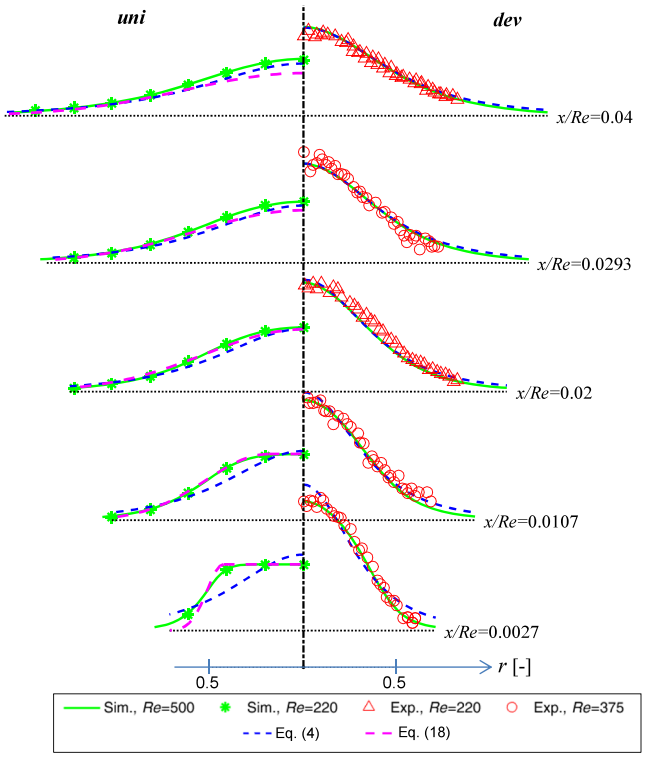

FIG. 13. Free-jet velocity profiles—numerical vs experimental results vs modified theory (Schlichting with virtual origin) and correlation (Martin).

between the boundary core length and momentum flux dictates that the self-similar solution should meet the approximate solution increasingly downstream with an increase in profile momentum flux (i.e., increasingly shorter virtual origin values).

Velocity profiles

Figure 13 shows a comparison for both the uniform and developed cases, between the current numerical and experimental results, the adapted correlation of Martin and the virtual origin modified theoretical solution of Schlichting. Validation of the numerical results for the developed case is clearly evident by comparison to the experimental results at five flight distances, over two Reynolds numbers, Re = 220 and 375. This figure also demonstrates the independence from Re when using the scaling of jet flight x/Re (Rankin and Sridhar, 1981), as numerical results at Re = 220 and 500 coincide (shown only for the uniform case) and experimental results at Re = 220 and 375 coincide with numerical results at Re = 500. It can also be seen that the modified correlation for the uniform profile, Eq. (18), captures the real profiles quite well in the range $0.005 \leq x/Re \leq 0.03$ (lower bound tested but not shown), beyond which the modified self-similar theory, Eq. (4) with virtual origins given by Eq. (22), predicts well for both profiles. In fact, for the fully developed case, the modified self-similar theory predicts to within 10% of the simulation profile already from $x/Re \geq 0.015$. Evidently, the most relevant range for practical applications falls within the boundary core, where highest inertia is available and at present is covered only for the uniform profile by Eq. (18). However, as shown in Fig. 14, the new approximate analytical solution extends the covered range to all profiles, at least within the boundary core.

Figure 14 shows the velocity profiles calculated using Eq. (11) compared to the numerical solution for the uniform (*uni*), partially developed non-monotonous (*par* 1), partially developed monotonous (*par* 2), and the fully developed (*dev*) issuing profiles. The solid black lines represent the domain where the difference between Eq. (11) and the numerical solution is smaller than 10% in value, whereas the black dotted lines represent the solution of Eq. (11) in the entire domain. Clearly, the approximate solution [Eq. (11)] is valid in the jet core region, thereby extending the range covered by existing models to all profiles, although with noticeable deviation at the jet radial edge and at the edge of the near-nozzle range (e.g., $x/Re \geq 0.028$ for a uniform profile). The reason for these deviations stem from the nature of the linearized convection diffusion approximation employed, which conserves mass while momentum decays, whereas the self-similar solution conserves momentum, while mass increases due to entrainment. While the latter represent the jet's *integral*

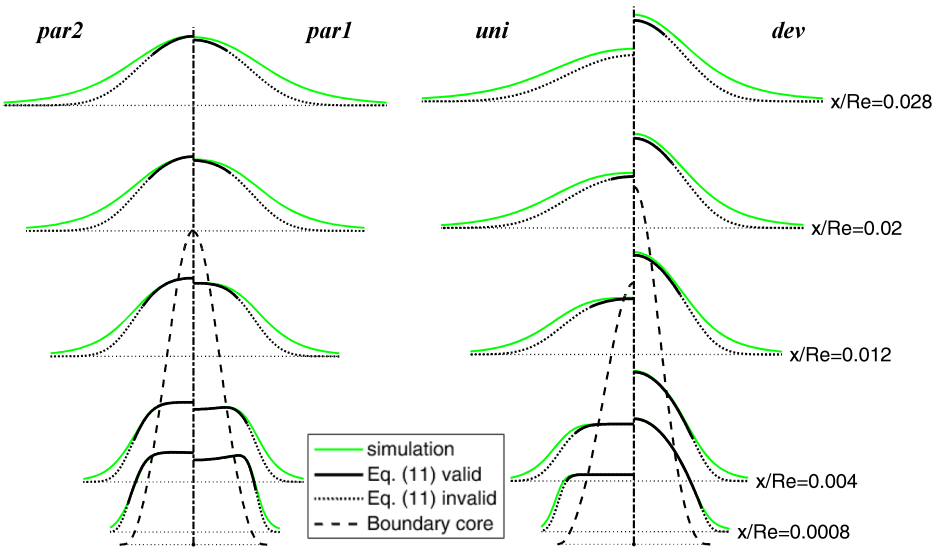

FIG. 14. Comparison of the linearized convection-diffusion solution [Eq. (11)] with the numerical solution for the uniform, partially developed, and developed issuing profile cases.

behavior more faithfully, within the *local* domain of the jet inner core, no entrainment occurs and momentum **does** decay due to profile relaxation (momentum transfer, away from the axis). Eventually, the deviations in the jet's outer core begin to significantly affect the inner core region, leading to increasing deviation beyond the near-nozzle region. Based on the observed criterion of 10% difference in value between the prediction and simulation, Fig. 14 shows that the boundary core contour for each issuing profile (shown in dashed lines) falls entirely within the approximate solution's valid region. This justifies its use for establishing both the potential and boundary cores.

In the light of this good agreement within the limited domain (shown in Fig. 14), we reconsider Eq. (11) and the linearization that led to it. For this, we evaluate the worst case scenario, i.e., the developed profile, in which the most significant initial deviations from the centerline (u_{per}) exist. For this case, initially about 1/3 of the jet diameter around the axis has a velocity within 10% of $u_{(0,0)}$. Moreover, the linearized term coefficient, $u_{(0,0)}$, here taken as a constant, decays slowly with x, losing less than 50% of its initial value over the near-nozzle region (or initially not at all for profiles with a potential core). By contrast, the derivative $(\partial u_{\text{per}}/\partial x)$ falls from **zero** to a finite negative value—a much more significant change. In the present approximation, the former was taken as a constant, whereas the latter is preserved. This may well explain the ability of the present approximation to predict the velocity evolution near the jet core.

Jet radial growth

Finally, in a fashion similar to the jet core, the jet radial extent (width), r_ϵ, can be defined with a cut-off value, ϵ, as

$$u(r_\varepsilon, x) = \varepsilon \cdot u(0, x). \tag{23}$$

Using Eq. (23) with a jet edge cut-off value of $\epsilon = 0.05$ [as in Kneer *et al.* (2014)], Fig. 15 compares the jet radial width from simulations, for three different profiles, with the asymptotic curve of the modified self-similar theory [Eq. (4)].

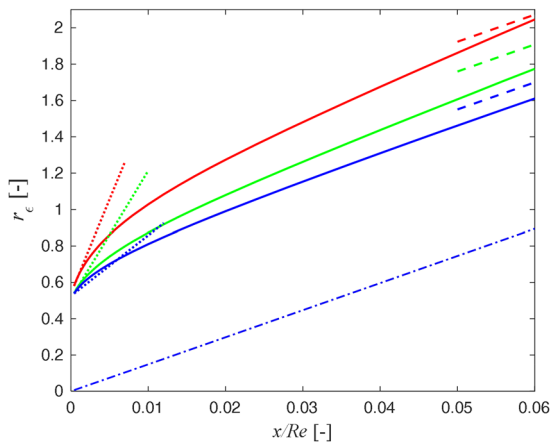

FIG. 15. Jet radial width for the uniform (red), partially developed (par 2, green), and fully developed (blue) cases during flight ($\epsilon = 5\%$). Dashed lines are asymptotes derived from Eq. (4); the dashed-dotted line is the jet width according to Eq. (4) with $\Delta x = 0$; dotted lines are initial widening asymptotes described in the text.

It is clearly seen from the figure that the uniform profile widens more rapidly than more developed profiles, similar to recent analytical and numerical findings (Revuelta *et al.*, 2002a and Uddin and Pollard, 2007). While the unmodified theory (Schlichting, 1967) captures only the downstream *slope* quite well, jet widths from simulations clearly converge within the near-nozzle range in *value* and *slope* to the modified theory. On the other extreme, near the nozzle in a recent analytical study (Revuelta *et al.*, 2002a), an *infinite* widening rate was implied, through a singularity in the entrainment rate at the nozzle exit plane. However, experimental studies have shown that the flow rearranges at the nozzle exit plane so as not to contain a singularity, giving a continuous transition rather than a true jump condition (Gear, 1983). Asymptotic analysis as $x/Re \to 0$ of the jet widening predicted by Eqs. (12) and (23) gives a *finite* jet widening rate seemingly similar to the numerical results and unique to each profile. However, as approaching the nozzle requires more and more terms in the series and the slope was found to be sensitive to the chosen criteria ($\epsilon = 0.05$ and minimal distance from nozzle—$x/Re = 2 \times 10^{-4}$), trends (dotted lines) are given for reference only and a more rigorous analysis is left for future study.

Jet widening has important implications to many fields, for example, flow near shear sensitive substances or the permitted proximity of adjacent jets in arrays for avoiding unwanted jet interaction (Herczynski *et al.*, 2004) or to the proximity of jets parallel to walls (Cabaleiro *et al.*, 2015).

CONCLUSIONS

A new approximate solution for submerged laminar jet flight was derived from a linearized convection-diffusion momentum equation, valid within the near-nozzle jet core region and for all archetypal issuing profiles. The validity of this solution was verified through detailed simulations and flow visualization experiments, over a wide range of conditions. Moreover, experimental findings support jet flight scaling according to x/Re, previously only shown numerically. While the developed approximate solution employing this scaling predicts the *centerline* velocity very well, its prediction of the entire jet *profile* evolution is not as accurate. Nonetheless, its accuracy in the core region and near the nozzle provides some novel insights into the jet core.

This analysis revealed analytically the actual shape of the potential core and its dependence on the issuing profile—inherently different from the common linear depiction. Furthermore, based on this analysis, a new "boundary core" was defined—the region still unaffected by the change in jet-edge shear upon emergence from the nozzle, although already subject to viscous profile relaxation. This new concept gives the minimal distance from the nozzle where self-similarity can begin to exist. Through the present analysis, this lower-bound for self-similarity (and use of the far-field theory) can be analytically determined, directly dictating the maximal permissible value for the virtual origin. Employing this modification, existing theory is brought into successful prediction of all relevant jet profiles' evolution already from the end of the boundary core, while the approximate solution predicts up to

there, where no previous analytical solution exists. This also allows the successful prediction of the asymptote of the jet radial width at the downstream edge of the near-nozzle domain, a matter of importance to several applications.

For prediction of only the centerline velocity decay, provided that the potential core length is known, a simple model is proposed. This model is based on an existing correlation for the developed issuing profile case and was here generalized to all profiles, and its constants were derived from physical considerations.

Alternatively for the mathematically more challenging case of a uniform profile, it is shown that the free parameters of an existing correlation can be unequivocally established by the present analytical method. This modified correlation captures the profile evolution already within the boundary core region.

ACKNOWLEDGMENTS

The authors would like to thank Professor Tuvia Miloh for his feedback on the article and the funding support from the Israel Science Foundation, Grant No. 4112/17.

APPENDIX A: NUMERICAL INDEPENDENCE TESTS

To verify the numerical model, a finer mesh consisting of 800 000 cells was used for the mesh independence test at $Re = 2000$ and for a uniform issuing profile, the case which involves the highest velocity gradients encountered in the entire parametric study conducted here.

To demonstrate the domain size independence of the conditions above, a case of reduced domain size was considered, where the radial size was reduced by 50%. The axial domain lengths were shortened from 10 jet diameters beyond the farthest profile examined (located 50 diameters downstream of the nozzle) to 5 diameters beyond. Figure 16 shows the independence test results, comparing velocity profiles at three flight distances ($x/Re = 0.0005$, 0.0025, and 0.025) for two mesh sizes and two domain sizes at the farthest flight distance, where the jet radial width is the largest and most affected by the proximity of the boundaries (the worst case scenario).

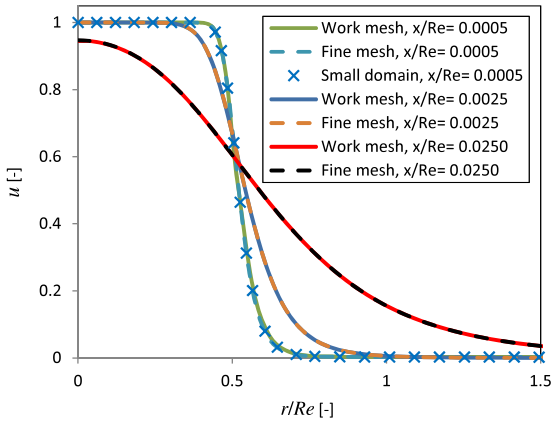

FIG. 16. Mesh and domain independence for the case of a uniform issuing profile at $Re = 2000$.

APPENDIX B: ANALYTIC SOLUTION VERIFICATION

The five different issuing jet profiles examined are approximated by the Fourier series, with coefficients given in Table I, for the analysis,

$$f_{uni}(r) = 1 - \text{uniform } (uni), \tag{B1}$$

$$f_{par1}(r) = a_0 + \sum_{n=1}^{6} [a_n \cos(n\omega r) + b_n \sin(n\omega r)]$$

$$-\text{partially developed } (par\ 1), \tag{B2}$$

$$f_{par2}(r) = a_0 + \sum_{n=1}^{3} [a_n \cos(n\omega r) + b_n \sin(n\omega r)]$$

$$-\text{partially developed } (par\ 2), \tag{B3}$$

$$f_{par3}(r) = a_0 + \sum_{n=1}^{2} [a_n \cos(n\omega r) + b_n \sin(n\omega r)]$$

$$-\text{partially developed } (par\ 3), \tag{B4}$$

$$f_{dev}(r) = 2(1 - r^2) — \text{ fully developed } (dev). \tag{B5}$$

TABLE I. Coefficients for the Fourier series representation of the partially developed profiles in Eqs. (B2)–(B4).

	$n = 0$	1	2	3	4	5	6
par 1							
a_n	0.7488	−0.0818	0.445 9	0.143 9	0.1207	−0.0826	−0.0259
b_n		0.9173	0.090 2	−0.030 5	−0.1421	−0.0888	0.0244
ω	8.309						
par 2							
a_n	0.8722	0.818	−0.332 50	0.049 02			
b_n		0.2508	−0.240 5	0.076 88			
ω	5.73						
par 3							
a_n	0.0769	2.073	−0.523 1				
b_n		0.0201	−0.02				
ω	3.68						

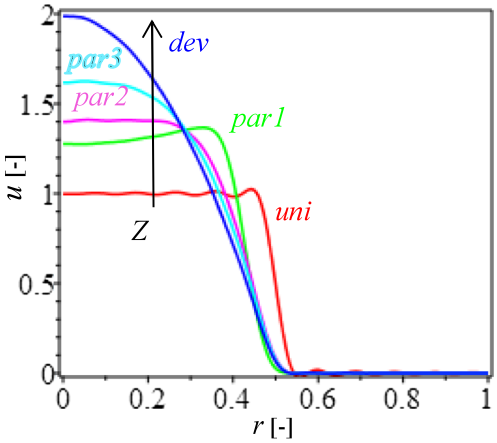

FIG. 17. Velocity profiles at $x = 0.1$ for the uniform (*uni*), partially developed 1 (*par* 1), partially developed 2 (*par* 2), partially developed 3 (*par* 3), and fully developed (*dev*) issuing profiles.

Figure 17 demonstrates the use of the solution given in Eq. (11) very near the exit from the nozzle ($x = 0.1$) for all issuing velocity profiles considered, with the series truncated at $N = 32$ ($n \leq 32$) and within a domain of radial size $B = 3/2$.

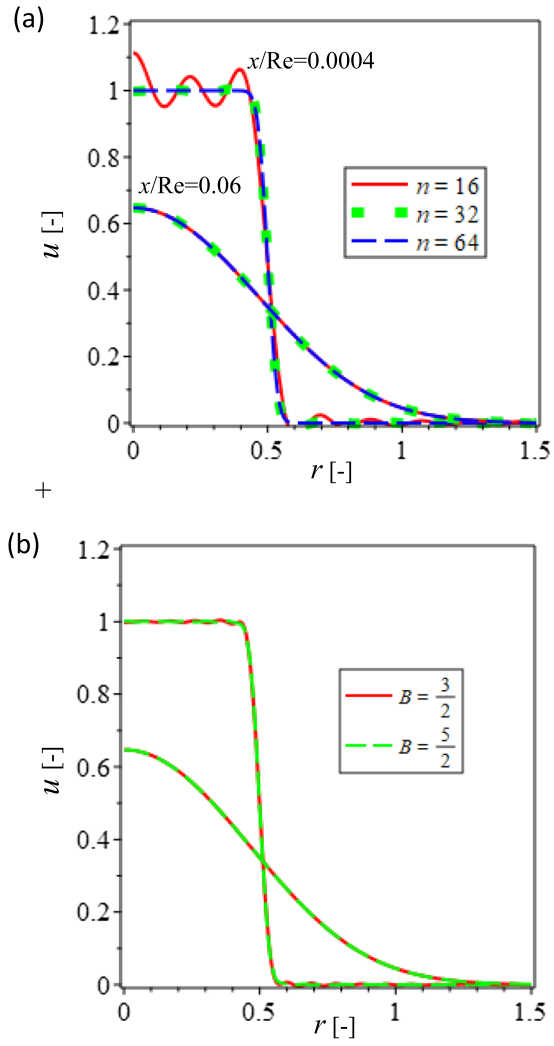

FIG. 18. Independence tests: velocity profiles for the uniform issuing profile at $x/Re = 0.0004$ and $x/Re = 0.06$ for the (a) number of terms and (b) radial domain size.

It is important to examine this approximate solution for all profiles very near the nozzle to verify its smooth and continuous behavior there with a truncation and a finite domain. Note that (1) the uniform profile is not as smooth as expected due to the limited ability to capture its large gradients by the truncated series ($N = 32$) and the radially large domain required for jet widening ($B = 3/2$) and (2) this method faithfully reproduces also the non-monotonous profile (*par* 1) obtained in a short nozzle.

To show that the chosen truncation and radial domain size is suitable to the entire studied set of conditions, independence tests were conducted as described in Appendix A. Figures 18(a) and 18(b) show the influence of variation of the number of terms in the series (N) and of the radial domain size (B), at two different axial locations for $Re = 500$. As the figure shows, sufficient accuracy is obtained in the domain of interest with $N = 32$ and $B = 3/2$. If the profile should be examined even closer to the nozzle, a larger N would be required, whereas for longer distances, B may have to be increased, although assumptions may not be valid there.

Agostini, B. *et al.*, "State of the art of high heat flux cooling technologies," Heat Transfer Eng. **28**(4), 258–81 (2007).
Akaike, S. and Nemoto, M., "Potential core of a submerged laminar jet," J. Fluids Eng. **110**, 392 (1988).
Allan, D., Caswell, T., Keim, N., and van der Wel, C., "Trackpy: Trackpy v0. 2.4," 2015, https://github.Com/soft-matter/trackpy/tree/v03.
Andrade, E. N. C. and Tsien, L. C., "The velocity-distribution in a liquid-into-liquid jet," Proc. Phys. Soc. **49**(4), 381–391 (1937).
Angioletti, M., Di Tommaso, R. M., Nino, E., and Ruocco, G., "Simultaneous visualization of flow field and evaluation of local heat transfer by transitional impinging jets," Int. J. Heat Mass Transfer **46**(10), 1703–13 (2003).
Atabek, B. H., Ph.D. thesis, University of Minnesota, Minneapolis, 1961, Retrieved (Dissertation Abstracts International, Vol. 22–06).
Cabaleiro, J. M., Laborde, C., and Artana, G., "Interaction between a laminar starting immersed micro-jet and a parallel wall," Phys. Fluids **27**(1), 013601 (2015).
Carlomagno, G. M. and Ianiro, A., "Thermo-fluid-dynamics of submerged jets impinging at short nozzle-to-plate distance: A review," Exp. Therm. Fluid Sci. **58**, 15–35 (2014).
Carslaw, H. S. and Jaeger, J. C., *Conduction of Heat in Solids*, 2nd ed. (Oxford University Press, Amen House, London, 1959).
Chung, Y. M., Luo, K. H., and Sandham, N. D., "Numerical study of momentum and heat transfer in unsteady impinging jets," Int. J. Heat Fluid Flow **23**(5), 592–600 (2002).
Cummings, E. B., "An image processing and optimal nonlinear filtering technique for particle image velocimetry of microflows," Exp. Fluids **29**(7), S042–S050 (2000).
Davies, J. M., Hutton, J. F., and Walters, K., "A critical re-appraisal of the jet-thrust technique for normal stresses, with particular reference to axial velocity and stress rearrangement at the exit plane," J. Non-Newtonian Fluid Mech. **3**(2), 141–160 (1977).
Donaldson, C. D. and Snedeker, R. S., "A study of free jet impingement. Part 1. Mean properties of free and impinging jets," J. Fluid Mech. **45**(2), 281–319 (1971).
Duda, J. L. and Vrentas, J. S., "Fluid mechanics of laminar liquid jets," Chem. Eng. Sci. **22**(6), 855–869 (1967).
Gear, R. L., "The shape of low Reynolds number jets," Phys. Fluids **26**(1), 7 (1983).
Glauert, M. B., "The wall jet," J. Fluid Mech. **1**(6), 625–643 (1956).
Grandchamp, X., Fujiso, Y., Wu, B., and Van Hirtum, A., "Steady laminar axisymmetrical nozzle flow at moderate Reynolds numbers: Modeling and experiment," J. Fluids Eng. **134**(1), 011203 (2012).
Greenshields, C. and Weller, H., "Implementation of semi-discrete, non-staggered central schemes in a colocated, polyhedral, finite volume framework, for high-speed viscous flows," Int. J. Numer. Methods Fluids **63**, 1–21 (2010).

Haustein, H. D., Harnik, R. S., and Rohlfs, W., "A simple hydrodynamic model of a laminar free-surface jet in horizontal or vertical flight," Phys. Fluids **29**(8), 082105 (2017).

Hennecke, D. K., "Heat transfer by Hagen-Poiseuille flow in the thermal development region with axial conduction," Wärme Stoffübertragung **1**(3), 177–184 (1968).

Herczynski, A., Weidman, P. D., and Burde, G. I., "Two-fluid jets and wakes," Phys. Fluids **16**(4), 1037–1048 (2004).

Incropera, F. P., Bergman, T. L., Lavine, A. S., and DeWitt, D. P., *Fundamentals of Heat and Mass Transfer*, 7th ed. (John Wiley and Sons, 2011), Retrieved (http://books.google.com/books?id=vvyIoXEywMoC&pgis=1).

Jambunathan, K., Lai, E., Moss, M. A., and Button, B. L., "A review of heat transfer data for single circular jet impingement," Int. J. Heat Fluid Flow **13**(2), 106–115 (1992).

Kashi, B. and Haustein, D. H., "Dependence of submerged jet heat transfer on nozzle length," Int. J. Heat Mass Transfer **121**, 137–152 (2018).

Kneer, R., Haustein, H. D., Ehrenpreis, C., and Rohlfs, W., "Flow structures and heat transfer in submerged and free laminar jets," in *Proceedings of the 15th International Heat Transfer Conference, IHTC-15* (Begell House Publications, 2014), pp. 497–517.

Lee, D. S., Kihm, K. D., and Chung, S. H., "Analytical solutions for the developing jet from a fully-developed laminar tube flow," J. Fluids Eng. **119**(3), 716 (1997).

Lienhard, J. H., "Heat transfer by impingement of circular free-surface liquid jets," in 18th National and 7th ISHMT-ASME Heat and Mass Transfer Conference 16, 2006.

Martin, H., "Heat and mass transfer between impinging gas jets and solid surfaces," Adv. Heat Transfer **13**, 1–60 (1977).

O'Neill, P., Soria, J., and Honnery, D., "The stability of low Reynolds number round jets," Exp. Fluids **36**(3), 473–483 (2004).

Olsen, M. G., "Depth of correlation reduction due to out-of-plane shear in microscopic particle image velocimetry," Meas. Sci. Technol. **21**(10), 105406 (2010).

Or, C. M., Lam, K. M., and Liu, P., "Potential core lengths of round jets in stagnant and moving environments," J. Hydro-Environ. Res. **5**(2), 81–91 (2011).

Rankin, G. W. and Sridhar, K., "Developing region of laminar jets with parabolic exit velocity profiles," J. Fluids Eng. **103**, 322 (1981).

Revuelta, A., Sánchez, A. L., and Liñán, A., "Confined axisymmetric laminar jets with large expansion ratios," J. Fluid Mech. **456**, 319–352 (2002a).

Revuelta, A., Sánchez, A. L., and Liñán, A., "The virtual origin as a first-order correction for the far-field description of laminar Jets," Phys. Fluids **14**(6), 1821–1824 (2002b).

Revuelta, A., Sánchez, A. L., and Liñán, A., "Confined swirling jets with large expansion ratios," J. Fluid Mech. **508**(508), 89–98 (2004).

Rohlfs, W. *et al.*, "Flow structures and heat transfer in submerged and free laminar jets," in *Proceedings of the 1st Thermal and Fluids Engineering Summer Conference, TFESC-1* (Begell House Publications, 2015), pp. 1011–1020.

Rohlfs, W., Ehrenpreis, C., Haustein, H. D., Garbrecht, O., and Kneer, R., "Influence of local flow acceleration on the heat transfer of submerged and free-surface jet impingement," in *Proceedings of the 15th International Heat Transfer Conference, IHTC-15* (Begell House Publications, 2014), pp. 3179–3192.

Rohlfs, W., Haustein, H. D., Garbrecht, O., and Kneer, R., "Insights into the local heat transfer of a submerged impinging jet: Influence of local flow acceleration and vortex-wall interaction," Int. J. Heat Mass Transfer **55**(25–26), 7728–7736 (2012).

Rosa, P., Karayiannis, T. G., and Collins, M. W., "Single-phase heat transfer in microchannels: The importance of scaling effects," Appl. Therm. Eng. **29**(17–18), 3447–3468 (2009).

Schlichting, H., *Boundary Layer Theory*, 7th ed. (McGraw-Hill Book Company, 1967).

Schmidt-Bleker, A., Reuter, S., and Weltmann, K. D., "Non-dispersive path mapping approximation for the analysis of ambient species diffusion in laminar jets," Phys. Fluids **26**(8), 083603 (2014).

Tropea, C. and Yarin, A. L., *Handbook of Experimental Fluid Mechanics* (Springer Science and Business Media, 2007).

Uddin, M. and Pollard, A., "Self-similarity of coflowing jets: The virtual origin," Phys. Fluids **19**(6), 068103 (2007).

Viskanta, R., "Heat Transfer to impinging isothermal gas and flame Jets," Exp. Therm. Fluid Sci. **6**, 111–134 (1993).

Watson, E. J., "The radial spread of a liquid jet over a horizontal plane," J. Fluid Mech. **20**(3), 481 (1964).

Webb, B. W. and Ma, C. F., "Single-phase liquid jet impingement heat transfer," Adv. Heat Transfer **26**, 105–217 (1995).

Wilson, D. E., "A similarity solution for the axisymmetric viscous-gravity jet," Phys. Fluids **29**(3), 632–639 (1986).

Zuckerman, N. and Lior, N., "Jet impingement heat transfer: Physics, correlations, and numerical modeling," Adv. Heat Transfer **39**(C), 565–631 (2006).